

## Daytime geomagnetic pulsations accompanying sudden impulse of solar wind

Tsegmed Battuulai<sup>1\*</sup>, Alexander Potapov<sup>2</sup>, Namuun Baatar<sup>1</sup>

<sup>1</sup> Department of Geomagnetism, Institute of Astronomy and Geophysics, Mongolian Academy of Sciences, Ulaanbaatar, Mongolia

<sup>2</sup> Department of near-Earth Space Physics, Institute of Solar-Terrestrial Physics of Siberian Branch of Russian Academy of Sciences, Irkutsk, Russia

ARTICLE INFO: Received: 12 May, 2022; Accepted: 27 Sep, 2022

**Abstract:** This article describes in detail ultra-low frequency (ULF) burst of oscillations, which was observed on April 23, 2002 immediately after a sudden geomagnetic pulse. The source of the pulse was a sharp inhomogeneity of the solar wind, which was acting on the magnetosphere, accompanied by a jump in dynamic pressure. We used simultaneous measurements of the magnetic and electric fields, as well as plasma parameters from the Polar satellite and data from induction magnetometers at the Mondy and Borok observatories. Polar spacecraft and obs. Mondy were near the noon meridian at the time of the burst recording. Comparing the time regime of dynamic spectra of oscillations on Earth and in space with on-board records of variations in the intensity and anisotropy of charged particles, we assumed that the burst of ion-cyclotron waves was excited as a result of the effect of a sudden impulse on the magnetosphere. The packet of these waves ran along the field line to the conjugate point in the ionosphere, and then propagated along the ionospheric waveguide. These conclusions are compared with another event on June 28, 1999, also associated with a sudden impulse. In this case, the form of the dynamic spectrum of the burst is characteristic not of ion-cyclotron, but of fast magnetosonic waves. Possible burst generation mechanisms of both types are discussed.

**Keywords:** ion-cyclotron wave; ultra-low frequency burst; charged particle flux; dynamic spectrum;

### INTRODUCTION

A sudden change in the dynamic pressure of the solar wind, affecting the magnetosphere, leads to the development of various oscillatory processes, which are observed in the magnetosphere in the form of magnetic oscillations, primarily, in the ultra low frequency (ULF) range [10, 18]. Electromagnetic ion cyclotron (EMIC) waves

are one of the manifestations of these wave processes. The main mechanism of EMIC wave generation in the magnetosphere is the cyclotron instability of the medium-energy ring current protons [4, 7] coming from the plasma sheet during an increase in magnetospheric convection.

\*corresponding author: [tseg@iag.ac.mn](mailto:tseg@iag.ac.mn)

<https://orcid.org/0000-0002-4828-8424>



The Author(s). 2022 Open access This article is distributed under the terms of the Creative Commons Attribution 4.0 International License (<https://creativecommons.org/licenses/by/4.0/>), which permits unrestricted use, distribution, and reproduction in any medium, provided you give appropriate credit to the original author(s) and the source, provide a link to the Creative Commons license, and indicate if changes were made.

In this case, a sharp growth in the solar wind dynamic pressure causes amplification in the thermal anisotropy of the magnetospheric plasma, which increases the growth rate of EMIC waves [14]. On the Earth's surface, these waves are recorded as Pc1 geomagnetic pulsations in the frequency range from 0.2 to 5 Hz. A number of authors divide Pc1s according to their spectral properties into two main types: structured quasi-sinusoidal oscillations ("pearls") and unstructured bursts [15]. The authors [8] were the first to carry out morphological study of the diurnal distribution of various types of hydromagnetic emissions in the Pc1 range at Syowa ( $L \sim 6$ ) station. Based on the type of registered spectral structures of more than 3000 events, the authors identified 8 different emission subtypes. One of the types of emissions found are burst-like structures that are observed in the daytime sector of the magnetosphere and correlate with sudden impulse (SI) events. As illustrated in Figure 6 by Fukunishi et al. [8], the emission frequency of this subtype (from 0.7 to 1.2 Hz on average) is higher as compared to other subtypes. The occurrence probability of the bursts is largest near magnetic local noon. These hydromagnetic emissions differ from classical Pi1B geomagnetic bursts (which are a high-frequency continuation of the broadband irregular PiB bursts and are associated with substorms) by the position of the daily maximum in the occurrence frequency, lower intensity, and significantly higher frequency.

The study [1] is dedicated to high-latitude ground-based observations of Pc1 pulsations in the Antarctica and Greenland ( $L \sim 7.5$ ), and simultaneous observation of ULF emissions on the Polar satellite. In 20 minutes after a strong increase in solar wind dynamic pressure (from 5 nPa to more than 20 nPa), the magnetometer on the Polar satellite registered two bursts, and quasi-structured emissions were observed around noon at stations in the Antarctica in the frequency range of 0.6–0.8 Hz. Moreover, the authors noted that bursts of Pi1 pulsations are observed at the moment of arrival of the solar wind pressure impulse.

Data analysis of synchronous observations from Van Allen probes and the Canadian network of magnetometers during the

recovery phase of a moderate geomagnetic storm [11] showed that the excitation of EMIC waves in the magnetosphere occurs in a very narrow ( $\Delta L \sim 0.1-0.4$  Re) latitudinal band of the inner magnetosphere ( $L \sim 4$ ) in the form of short-term narrow-band emission. The ground-based network of magnetometers at that time registered long structured oscillations, the so-called "pearls". Comparing three identical events from satellite and ground-based observations, Pilipenko et al. [16] concluded that the ion-cyclotron instability does not develop continuously, but in a pulsating regime with a characteristic cycle time of up to  $\sim 10$  min. These studies refer to EMIC waves generated in the magnetosphere during the recovery phase of a magnetic storm, as a rule.

Most of the published works that have studied the excitation and propagation of EMIC waves in the magnetosphere deal with events observed either during quiet times in the inner magnetosphere or during disturbances (geomagnetic storms and substorms) on the night side. Much less attention has been paid to EMIC-related processes occurring in the noon sector near the magnetopause. But it is there that wave processes can occur, including in the EMIC range, affecting the transfer of energy from solar wind to magnetosphere through wave-particle interaction and the occurrence of turbulence. Such processes are especially probable at times of sharp increases in the pressure of solar wind on the magnetosphere. In this regard, in this article, we set ourselves the goal of studying in detail the conditions under which EMIC bursts occur in the near-noon region of the magnetosphere, using both ground-based and satellite data.

Here, we examine short-term ULF emissions in the daytime sector of the magnetosphere at the moment of the magnetopause contact with the front of an interplanetary shock wave. These events differ from those previously considered by other authors in that the appearance of burst-like ULF emissions in the frequency range of 0.1–3.0 Hz did not occur against the background of the recovery phase or the expansion phase of a magnetic storm. We were interested in the moment of sudden impulses SSC (Sudden Storm Commencement) or SI after a prolonging

quiet geomagnetic period, so that other processes in the excitation of bursts would not affect, except for an isolated impulse.

The main objective of this work is to carry out a comparative study of bursts of geomagnetic pulsations observed in the daytime magnetosphere and at the mid-latitude

## MATERIALS AND METHODS

Our study of burst-like ULF emissions is based on synchronous observation of the geomagnetic field on the Earth, the electromagnetic field and plasma in the magnetosphere and in interplanetary space. All satellite data are taken from the Coordinated Data analysis web ([https://cdaweb.gsfc.nasa.gov/istp\\_public/](https://cdaweb.gsfc.nasa.gov/istp_public/)). CDAWeb contains selected public non-solar heliophysics data from current heliophysics missions and projects.

According to the bulletins of geomagnetic indices, SSC or SI events were selected, during which obs. Mondy was near geomagnetic noon. For detailed analysis, IMF values, solar wind parameters and geomagnetic indices were selected prior to the event of April 23, 2002 before they were disturbed by the sudden sharp enhancement in solar wind pressure, i.e., when the geophysical condition was quiet. Additionally, when discussing the results, the event of June 28, 1999, occurred against a quiet geomagnetic background, will be considered. The choice of quiet conditions allows us to believe that a key role in the excitation of geomagnetic pulsations was played by a sudden impulse caused by the contact of the solar wind inhomogeneity with the Earth's magnetosphere.

The characteristics of the solar wind plasma and the interplanetary magnetic field (IMF) were studied, using data from the SWE (Solar Wind Experiment) and MFI (Magnetic Field Instrument) instruments installed on the ACE (Advanced Composition Explorer) satellite. ACE orbits the L1 libration point, which is a point of Earth-Sun gravitational equilibrium about 1.5 million km from Earth and 148.5 million km from the Sun. The exact coordinates of this spacecraft during the April 23, 2002 event are shown below.

ground-based observatories, at the moment of a sharp increase in the solar wind dynamic pressure. Spectral structure analysis of these pulsations will be performed and a discussion about possible source of their generation will be presented.

The properties of hydromagnetic emissions on the ground were analyzed using digital data from induction magnetometers (sampling frequency 10 Hz) installed at the Mondy ( $\Phi = 47^\circ$ ,  $\Lambda = 174^\circ$ ,  $L = 2.2$ ), Borok ( $\Phi = 54^\circ$ ,  $\Lambda = 113^\circ$ ,  $L = 2.9$ ), and Lovozero ( $\Phi = 64^\circ$ ,  $\Lambda = 115^\circ$ ,  $L = 5.2$ ) observatories (corrected geomagnetic coordinates are indicated). During the events under consideration, identical magnetometers operated at the Mondy and Borok observatories.

We used data from the following 4 instruments installed on the Polar satellite in order to investigate hydromagnetic emissions observed in the daytime magnetosphere:

1. Ion hot plasma instrument HYDRA (a three-dimensional electron with energies between 10-19 keV, sampling step  $\Delta t = 13.8$  s [18]);
2. The electric field instrument (EFI) (vector electric field, measurement with  $\Delta t = 0.05$  s; in the National Space Science Data Center data are exposed with resolution 1 data point about every 6 seconds ( $\Delta t = 6$  s) [9]);
3. Thermal Ion Dynamics Experiment (TIDE) instrument (thermal/superthermal ion population from 0.32 to 410.62 eV,  $\Delta t = 6$  s, [13]);
4. The MFI - three components of the high-resolution magnetic field vector with  $\Delta t = 0.12$  s (represented in satellite coordinate system) and of low resolution  $\Delta t \approx 6$  s (in GSM coordinate system) [17]).

For comparison with ground-based observations, Polar satellite magnetic data with a time resolution of 0.12 s are interpolated by a cubic spline with sampling rate of  $\Delta t = 0.1$  s, which is equivalent to the sampling rate of ground-based magnetic data.

The electric and magnetic field measured data on the Polar satellite are presented in the satellite coordinates. Converting algorithm of these measurements to the GSM coordinate system is given in the Appendix.

The spectral structure of the magnetic field variations was studied by the Fourier transform with 0.1 s time resolution of the initial ground and interpolated satellite data. The fluctuation spectrum of ULF emissions was in the frequency range 0.5–2.0 Hz. Emissions were filtered using a digital filter based on an algorithm that does not distort the phase characteristic of the original signal [12].

## RESULTS AND DISCUSSION

### *Geophysical conditions during the April 23, 2002 event*

On April 23, 2002, during the sudden impulse of the solar wind dynamic pressure, obs. Mondy was near geomagnetic noon (11:14 MLT (Magnetic Local Time)), and the Polar satellite was 9.5 arc degrees west (10:36 MLT) of the geomagnetic field line with  $L = 8.7$  at a point with coordinates  $X_{GSM}, Y_{GSM}, Z_{GSM} = 4.16, -1.49, 3.19$  Re (Earth radius), respectively. The geographic coordinates of the foot of the geomagnetic field line passing through the satellite ( $\varphi = 75.19^\circ$  N,  $\lambda = 82.61^\circ$  E) were determined using the program posted on the website <https://sscweb.gsfc.nasa.gov/cgi-bin/CoordCalculator.cgi>.

A discontinuity in the solar wind at 04:14 UT, the ACE satellite ( $X = 224.4$  Re;  $Y = 27.8$  Re;  $Z = -22.7$  Re) was registered, at the leading edge of which the density  $N_p$  of the solar wind increased sharply from  $\sim 5$  to  $\sim 17$   $\text{cm}^{-3}$ , and the velocity  $V_{sw}$  from  $\sim 400$  to  $\sim 600$  km/s, which corresponded to an increase in dynamic pressure from 2 to 10 nPa. The jump in  $N_p$  and  $V_{sw}$  was accompanied by an increase in IMF from 8 to 20 nT.

To move from these data to the situation at the magnetosphere boundary, we used the

The method used in our study was to reconstruct the time history of the appearance of EMIC bursts in the magnetosphere and on the Earth's surface against the background of variations in ion fluxes and longitudinal electric field. At the same time, variations in the parameters of the solar wind and the interplanetary magnetic field were monitored, and their influence on the generation of EMIC bursts was estimated. Next, the dynamic spectra of the emissions observed on the satellite and on the ground were constructed, and based on their comparison relevant conclusions were drawn about the propagation paths of the oscillations.

results presented at the OMNI website. OMNI data center, using the measurements of spacecraft located near the libration point L1, recalculates them to values approximately corresponding to the parameters before the front of the near-Earth bow shock. (The transformation details can be found in [[https://omniweb.gsfc.nasa.gov/form/omni\\_min.html](https://omniweb.gsfc.nasa.gov/form/omni_min.html)]). Figure 1 shows that according to the 1-minute OMNI data, there was a sudden increase in the solar wind push, at the leading front of which the density  $N_p$  rose sharply from  $\sim 4$  to  $\sim 16$   $\text{cm}^{-3}$  (fourth plot from the top), and the velocity  $V_{sw}$  from  $\sim 400$  to  $\sim 600$  km/s (third plot from the top), which corresponded to magnification in dynamic pressure from 1 to 11 nPa (third plot from the bottom). The jump in  $N_p$  and  $V_{sw}$  was accompanied by an increase in the IMF from 6 to 16 nT (the top plot). Before the solar wind pressure increase, the  $B_z$  component (second plot from the top) of the IMF was positive and did not experience strong jumps, but in 1.5 minutes after the sharp growth in pressure, it became negative ( $B_z < 0$ ). Also, the beta parameter had a dramatic increase (the bottom plot).

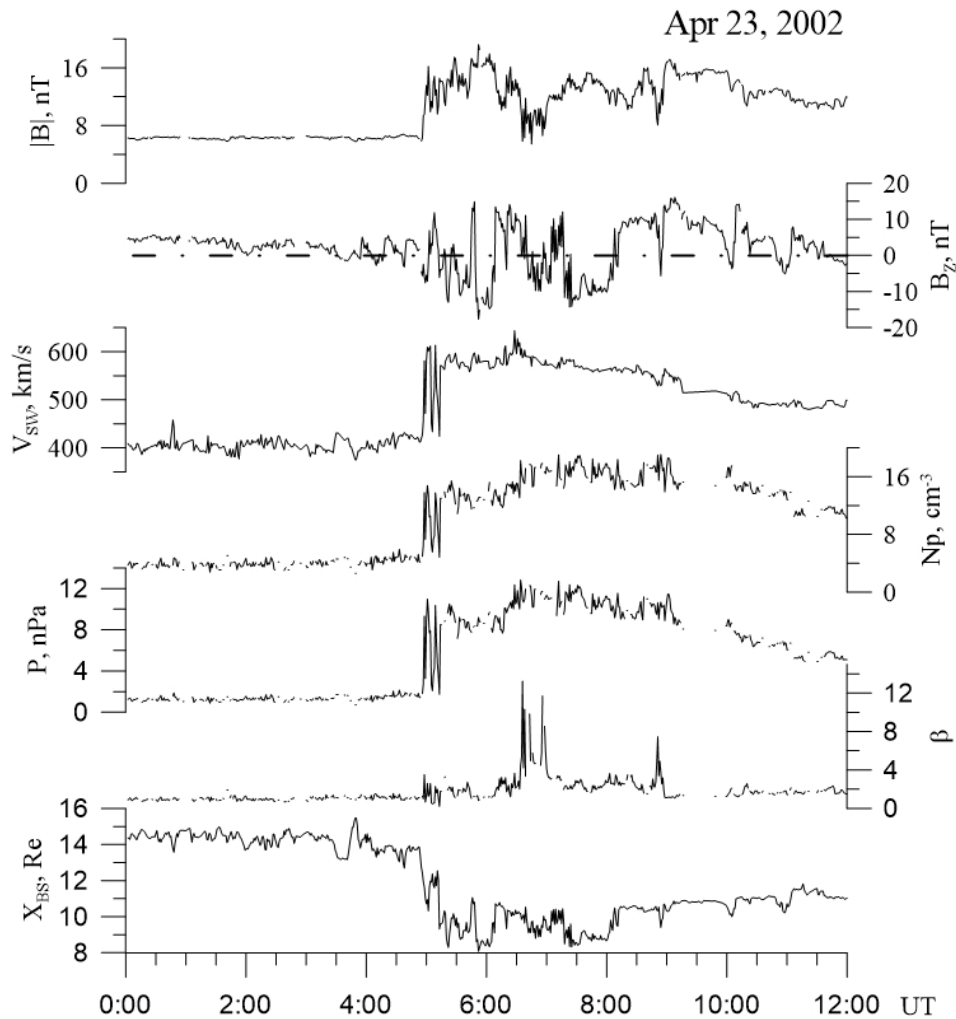


**Figure 1.** The conditions in near-Earth space environment for the April 23, 2003 event from OMNI data. From the top to the bottom, panels show magnitude of the IMF ( $|B|$ ), vertical component of the IMF ( $B_z$ ), solar wind velocity ( $V_{sw}$ ), proton density ( $N_p$ ), solar wind dynamic pressure ( $P$ ), beta parameter of plasma ( $\beta$ ), bow shock displacement of the near-Earth shock wave ( $X_{BS}$ )

Figure 2 shows variations in the SYM-H index representing intensity of the symmetric part of the Earth’s ring current, a discontinuity in the solar wind initiated a moderate magnetic storm at 04:48 UT with SSC (there was a sharp jump in the SYM-H index by approximately 55 nT for 4 min, followed by a gradual decrease in SYM-H to  $-80$  nT). During SSC, the AE index of auroral activity sharply amplified from 80 to

580 nT, after which it grew to 1600 nT over the next two hours. Before the moment of SSC, since the beginning of the day, the SYM-H index remained almost unchanged, and the AE index did not exceed 100 nT.

Thus, this SSC event developed against the background of a quasi-stationary weakly enhanced ring current and low auroral activity.

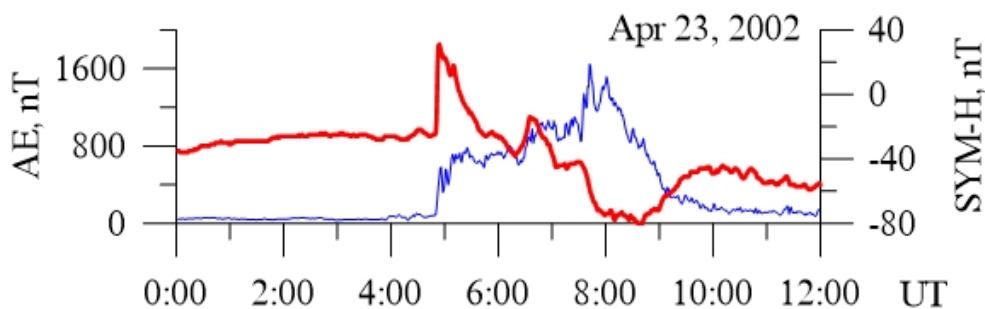


**Figure 2.** Variations in SYM-H (red line) and AE (blue line) indices

**High frequency ULF disturbances**

At 04:48 UT the Polar satellite was located in the daytime magnetosphere on the field line with geomagnetic coordinates  $\Phi = 70.08^\circ$ ,  $\Lambda = 158.25^\circ$ . According to data from

the Polar, the solar wind pressure impulse excited short-term broadband oscillations in the Earth's magnetosphere, against which bursts of high-frequency pulsations were observed (Fig. 3).

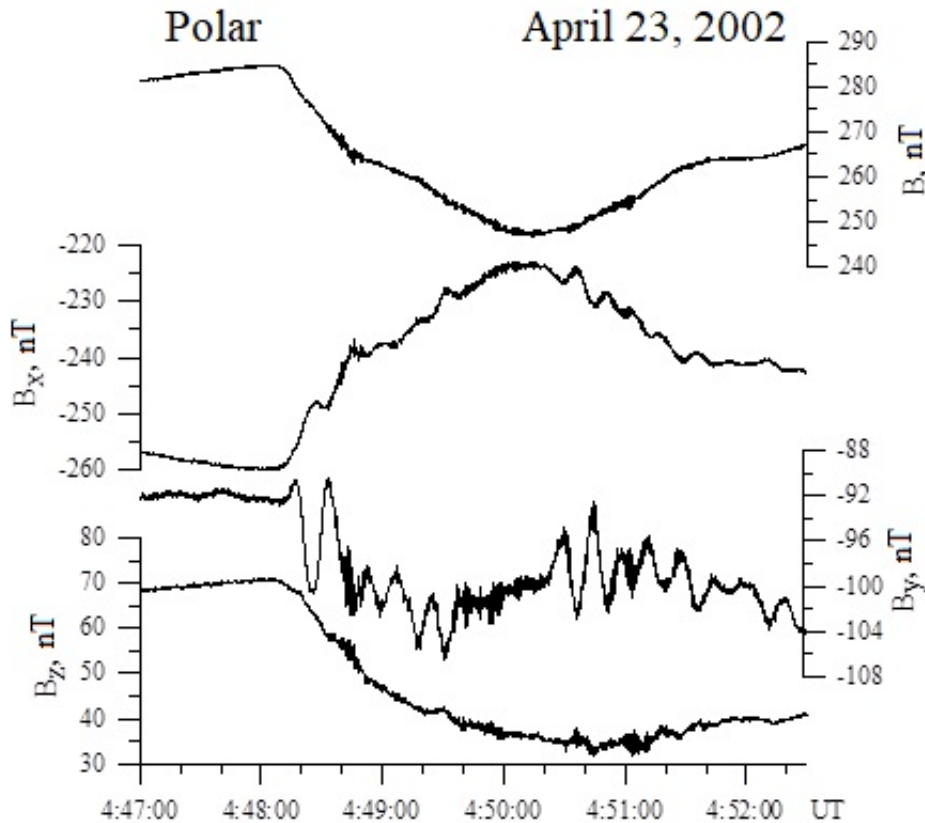


**Figure 3. Magnetic field fluctuations recorded by the Polar satellite. Field components are shown in satellite coordinate system (see the coordinate description on the site [http://www-ssc.igpp.ucla.edu/forms/polar/ascii\\_full.html](http://www-ssc.igpp.ucla.edu/forms/polar/ascii_full.html))**

Figure 4 shows the dynamic spectra of the ULF oscillations recorded at the Mondy observatory (the bottom spectrum) and by the inductive magnetometer on-board of the Polar (the top spectrum). We see that in 30 seconds after the beginning of the sudden impulse, high-frequency ULF disturbances were recorded both by the satellite and on the ground. They had similar spectral composition, but with a different shape of dynamic spectrum. The structure presented in the dynamic spectrum of Polar consists of two sharp vertical bursts occupying the frequency band of 0.6–1.4

on and a relatively narrow-band emission whose frequency increases over time. The presence of these three structures can also be seen in the bottom panel of Fig. 5, which shows variations in the Bx component of the magnetospheric magnetic field in the 0.6–1.4 Hz frequency band. They are extracted from satellite magnetic data using their interpolation with a Marmet bandpass filter. The average frequency of local spectral maxima increases as the ULF disturbance develops, thus forming a signal of increasing frequency.

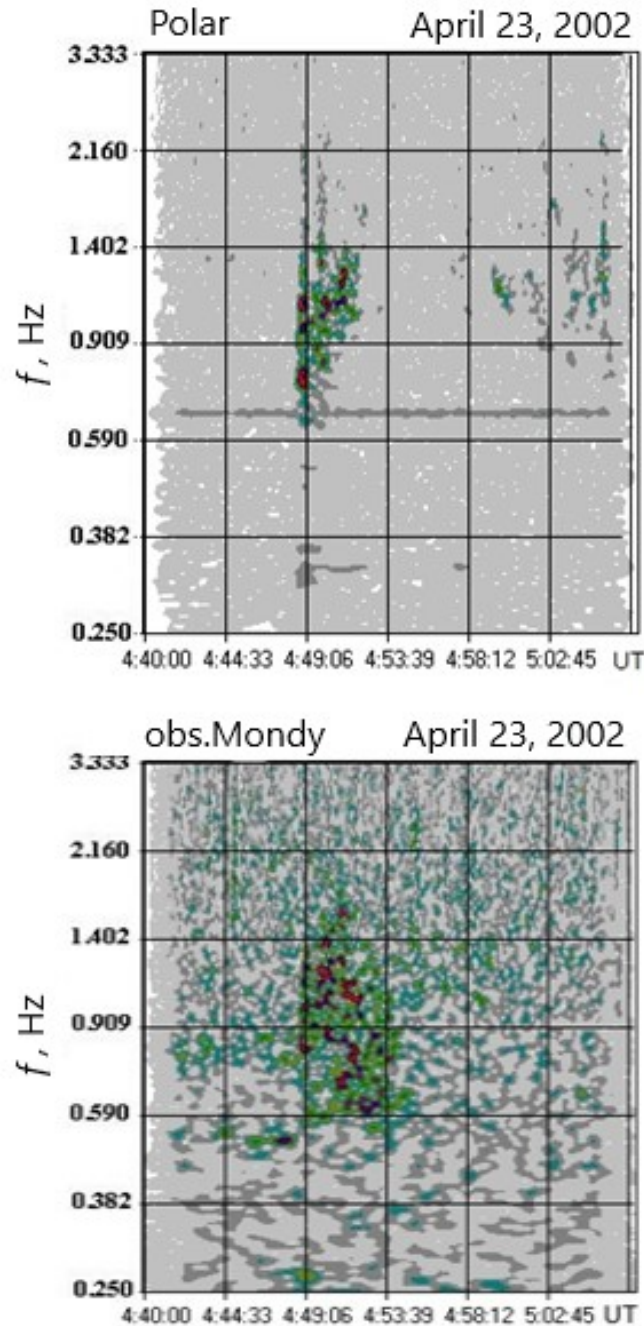


**Figure 4. Dynamic spectrum of the ULF emission recorded by magnetometers on the Polar satellite and obs. Mondy**

For this rare case, when the satellite was near the noon meridian at the moment of shock wave arrival, obs. Mondy was located nearby noon sector ( $LT \approx 11:40$ ). A noise signal can be seen from dynamic spectrum of the obs. Mondy on the same frequencies of 0.6–1.4 Hz. The time of this signal almost coincides with the beginning of the first ULF burst at Polar. In contrast to the pulsations observed in the magnetosphere, the high-frequency ULF

emission on the ground is longer. In the first two minutes, the dynamic spectrum of the ground-based emission resembles the spectrum of the emission observed on the satellite: two vertical lines are noticeable, but they are much more blurred and had a slight positive slope to the time axis. Later, the frequency structure is smeared and the emission amplitude maximum shifts down.

*A linkage of bursts to the magnetospheric parameters*

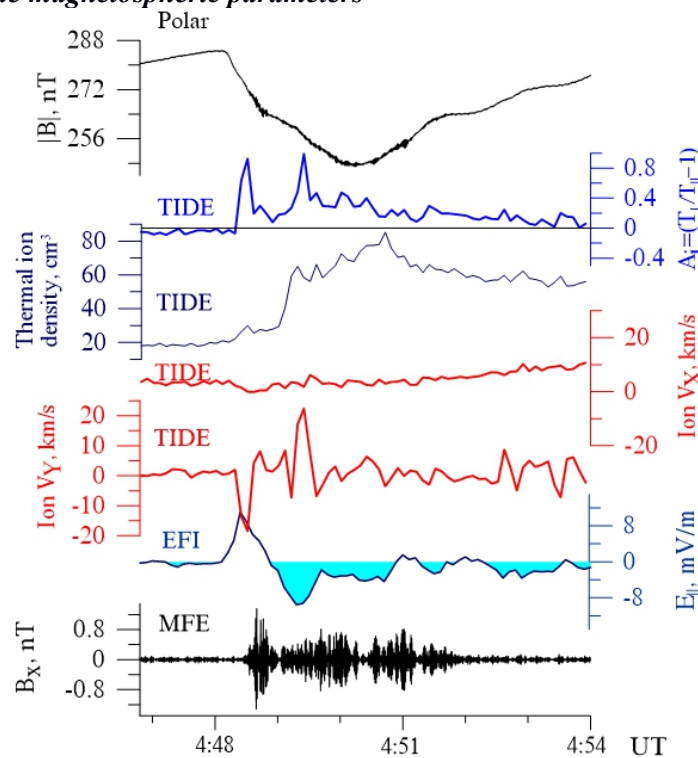


**Figure 5.** Time series of parameters and magnetospheric field recorded by the instruments on the Polar satellite. From top to bottom: magnetic field magnitude ( $|B|$ ), calculated anisotropy of ion temperature ( $A$ ), the density of thermal ions and their transverse velocities ( $V_x$ ,  $V_y$ ) relative to the magnetic field, converted longitudinal electric field ( $E$ ), high-frequency filtered  $B_x$  component of the magnetic field

Figure 5 illustrates a comparison of the time series of the main geomagnetic field (the top plot) and the filtered high-frequency part of the MFE-measured magnetic field in the magnetosphere (the bottom plot) with the environmental parameters recorded by different instruments located on the Polar satellite: anisotropy  $A = T_{\perp}/T_{\parallel} - 1$  ( $T_{\perp}$  and  $T_{\parallel}$  are ion temperature across and along geomagnetic field) of thermal ions calculated from TIDE measurements (second plot from the top), thermal ion density and velocities along X and Y axis (third to fifth plot from the top), all measured with TIDE, and the longitudinal electric field measured by EFI.

The magnetic field strength begins to decrease (first panel from the top) at the onset moment of a sharp increase in the solar wind dynamic pressure. Simultaneously, the amplification of the electric field components directed along the external magnetic field begins (second panel from the bottom). Due to the impulsive action of the solar wind, an abrupt jump in the anisotropy of thermal ions occurred

(second panel from the top). Anisotropy arises when thermal ions "rocked" in the azimuth direction, moving first in one direction and then in the other, as shown in the third panel from the bottom. In this case, the ion velocity in the radial direction does not change. The ion density, shown in the third panel from the top, begins to gradually grow, but with the second sharp increase in anisotropy, it also sharply rises and reaches a maximum at about 4:48:30 UT. At this time, the direction of the longitudinal electric field abruptly changes to the opposite, i.e., it is set against the direction of the main magnetic field. Note that the electric field research instrument is designed to register the field only in the low-frequency region.

We studied daytime Pc1 geomagnetic emissions that were observed after SSC, using data from the Polar satellite and on-ground induction magnetometer in the Mondy observatory both being located in the vicinity of the noon meridian at the moment of the SSC.

We believe that the observed emissions are electromagnetic ion cyclotron (EMIC) waves.

EMIC waves are generated in the magnetosphere due to the resonance cyclotron instability of ring current ions with temperature anisotropy. Olson et al. [14], using a simple model describing the change in the characteristics of the daytime magnetospheric plasma, showed that sudden increases in the solar wind dynamic pressure can cause bursts of ULF emissions near the local noon. A dramatic compression of the magnetosphere due to an increase in solar wind pressure causes the maximum distortion of the magnetospheric plasma around noon at high latitudes [14] leading to sudden increase of thermal anisotropy of the ring current ions. This, in turn, increases the increment of the ion-cyclotron instability and amplifies excited EMIC waves. This picture is consistent with the results of observations made on the Polar satellite for the April 23, 2002 event. Figure 5 demonstrates that, namely, the sharp jump of solar wind pressure led to the dramatic acceleration of thermal plasma ions, whose velocity reached 20 km/s in the azimuth direction. Together with a jump-type growth in the azimuthal velocity of the thermal plasma, a significant increase in temperature anisotropy occurs synchronously up to the maximum value  $A = 1$ . The generation of ULF bursts begins 30 sec after the arrival of SI, demonstrating that wave-particle interaction occurs on the field lines near noon.

The further emission development correlates with a gradual rise in the plasma density shown in the third panel from the top in Figure 5. This gradual increase, i.e., the injection of ions into the magnetosphere, takes place against the background of a continuing growth in the anisotropy  $T_{\perp} > T_{\parallel}$  of the distribution of ions, which, in turn, preserves the conditions for the excitation of the EMIC waves by their cyclotron resonance with ions, which is the main mechanism for generating these waves (see [4, 19] and references therein).

At the same time, the longitudinal electric field is enhanced, first against and then in the direction of the external magnetic field; direction of the electric field changes approximately in antiphase with the azimuthal velocity of thermal ions.

### ***Localization and observation on earth's surface***

It is known that the EMIC waves propagate in the magnetosphere mainly along geomagnetic field lines, they penetrate through the ionosphere to the Earth's surface, and are observed in the form of Pc1 geomagnetic pulsations. At ionospheric heights, these waves are partially transformed into magnetosonic waves, which propagate along the earth's surface over long distances in the so-called ionospheric MHD waveguide.

Observations carried out on several satellites indicate a narrow localization of EMIC wave sources and their channeled propagation along the geomagnetic field [11, 16]. Based on the results of these studies, it can be assumed that the burst of ULF emission generated around noon at the moment of a sudden pressure impulse and it was observed on the Polar satellite and in the obs. Mondy (Fig. 5), should have propagated from the magnetosphere to the polar ionosphere along the geomagnetic field line with  $L \sim 8-9$ , and further run along the ionospheric waveguide to obs. Mondy ( $L = 2.2$ ).

### ***Spectral structure***

In the event under consideration, the first two structural elements of the ULF burst on the spectrograms are located vertically on the Polar satellite and with a slight positive slope with respect to the time axis at the Mondy observatory (rising frequency change). This fully corresponds to the frequency dispersion of ion-cyclotron waves propagating from a source located in the magnetosphere along the field line to the ionosphere. The third element on the Polar spectrogram (the top panel of Figure 4) has a clear positive slope. Possibly, it corresponds to the reflection of the second impulse from the ionosphere. However, this type of structure is not always observed. According to obs. Syowa (Antarctica) [8] near noon, after a sudden impulse of solar wind pressure, bursts are generated with a vertical spectral structure with frequency of about 1 Hz and higher.

Nevertheless, at obs. Mondy, under the same conditions, bursts of pulsations are sometimes observed, which have a descending spectral structure.

The results of observations of two events from data of the mid-latitude observatories Mondy and Borok, as well as the subauroral observatory Lovozero [20], show a noticeable descending, or falling structure of wave packets accompanying SI. Dynamic spectra of one of the events observed on June 28, 1999 is shown in Figure 6, where one station (Mondy) was located around noon, and the other two (Borok

and Lovozero) were in the morning sector. The spectra were plotted from magnetic measurements at these three observatories equipped with induction magnetometers. There are no satellite data for this event around noon, so we could not compare the spectral characteristics of bursts in the magnetosphere and on the Earth's surface.

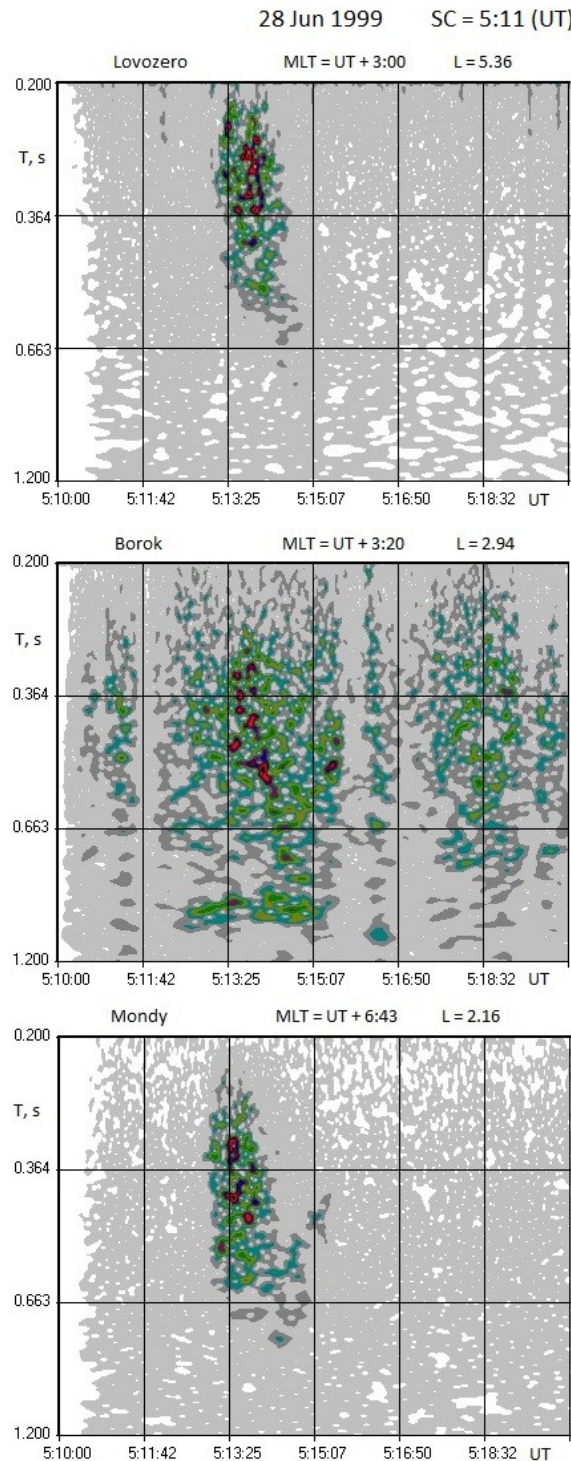


**Figure 6. Dynamic spectrum of ULF emission of the June 28, 1999 event. From top to bottom: obs. Lovozero, Borok and Mondy**

The descending shape of the structural elements of the burst dynamic spectrum suggests that the high frequencies of the burst propagate faster than the lower frequencies. Frequency dispersion of this kind can be conventionally called R-mode dispersion, since, for example, it is characteristic of fast magnetosonic waves with right-hand polarization propagating along an external magnetic field (R-waves). However, this dispersion is not typical for EMIC waves. They have left-hand polarization (L-mode) when propagating along the magnetic field, and the higher-frequency ion-cyclotron waves propagate more slowly than the low-frequency ones, which lead to a positive slope of the structure patterns in the EMIC dynamic spectrum. Therefore, it remains unclear how the descending elements of the dynamic spectrum structure could be formed.

One of the possible options may be the mechanism proposed in [6]. The authors found cases of ground-based observations of structured emissions in the Pc1 range with an unusual frequency dispersion of discrete elements: they had a negative slope to the time axis on the spectrogram, that is, a descending structure characteristic not for the L-mode, but for the R-mode, located on the same branch of the dispersion equation with fast magnetic sound. To explain their observations [6] have invoked model of R-wave generation by a longitudinal proton beam with an energy of 10–100 keV.

It is quite possible that a similar mechanism worked in the event of June 28, 1999, if we assume that the sudden compression of the magnetosphere somehow launched a longitudinal proton beam in the region of magnetic shells  $L \sim 6-7$ , in the longitudinal sector  $MLT \sim 10-12$  hours, where a sharp increase in the ion flux was recorded on the

## CONCLUSIONS

We found that the impact on the magnetosphere of an impulse caused by a sharp inhomogeneity of the solar wind can lead to the excitation of two ULF bursts of different nature in the daytime magnetosphere. In one case, this

LANL-1994 and, a little later, on the LANL-97 satellites [20]. Almost simultaneously with this, a burst of emission was observed at the obs. Mondy, and 12 s later, at the Lovozero-Borok meridian (Fig. 6, see also [20]).

Note that for the two cases of Pc1 pulsations analyzed in [6], the use of this mechanism looks unconvincing, since the generation of pearl pulsation series requires multiple runs of wave packets between conjugated ionospheres along the field line, and R-waves, in contrast to ion-cyclotron L-waves, are not channeled by the magnetic field. Another mechanism for the appearance of emissions with downward dispersion can be the excitation of ion-cyclotron L-waves in a multicomponent plasma discussed in the same article [6] with their subsequent transformation into R-waves on their way to the Earth's surface along the field line. This effect was considered theoretically in work [5].

One more source of frequency dispersion, leading to the appearance of a descending signal structure in the dynamic spectrum, is the waveguide dispersion considered for the ULF range in [2, 3]. Its appearance requires signal propagation in the form of a fast magnetosonic wave in a waveguide formed by a large-scale plasma inhomogeneity. An example of such an inhomogeneity is the plasma sheet in the magnetotail. However, in our case it is difficult to imagine the existence of the required structure in the dayside magnetosphere.

The possible development of the research started in this article can lie in two directions. On the one hand, this is the development of the theory in an attempt to explain the mechanisms of generation and propagation of the studied ULF emissions, and on the other hand, the involvement of new satellite and ground-based observations for detailing and, possibly, statistical analysis of the phenomenon.

is a burst of EMIC waves with their characteristic L-dispersion, and in the other case, a burst of ULF waves of an unknown nature with R-dispersion. To explain the second

case, we have proposed three different possible mechanisms.

**Acknowledgments:** The authors are grateful to the curators of the CDAWeb and UCLA project for providing open access to Polar satellite data as well to R.A. Rakhmatulin and A.G. Yakhnin for making available their digital data of obs. Mondy and Lovozero. The study was carried out with partial financial support from the Geomagnetic Department of the Mongolian Academy of Sciences. Contribution of A.S.P.

**Appendix**

The electric field in the Polar data is represented as two orthogonal components lying in the satellite rotation plane (spin plane). These components are the  $E_{XY}$  component directed along the line of intersection of the spin plane (it is assumed that it coincides with the plane of the orbit) with the plane of the ecliptic and the  $E_Z$  - component perpendicular to the  $E_{XY}$  - component. Components  $E_{XY}$  and  $E_Z$  are positive in the antisolar and northern directions, respectively. The angles of declination of the

was financially supported by the Ministry of Science and Higher Education of Russia. This work is a continuation of the cycle of joint Mongolian-Russian research in the field of studying magnetospheric phenomena in their connection with space weather, as well as with seismic activity. Cooperation was started at the end of the last century within the framework of the Joint Soviet-Mongolian geophysical expeditions. The results achieved are reported and discussed at regular bilateral scientific conferences.

satellite spin vector to the  $XOY_{GSM}$  ( $\Theta$ ) plane and right ascension ( $\Phi$ ) of the spin vector projection onto the  $XOY_{GSM}$  plane relative to the  $OX_{GSM}$  axis indicated in the Polar data allows to convert the electric field vector to the geomagnetic solar-magnetospheric coordinate system GSM, and then calculate its longitudinal and transverse relatively smoothed magnetic field components.

Illustration explaining the values of the oriented angles  $\Theta$  and  $\Phi$  are shown in Fig A1

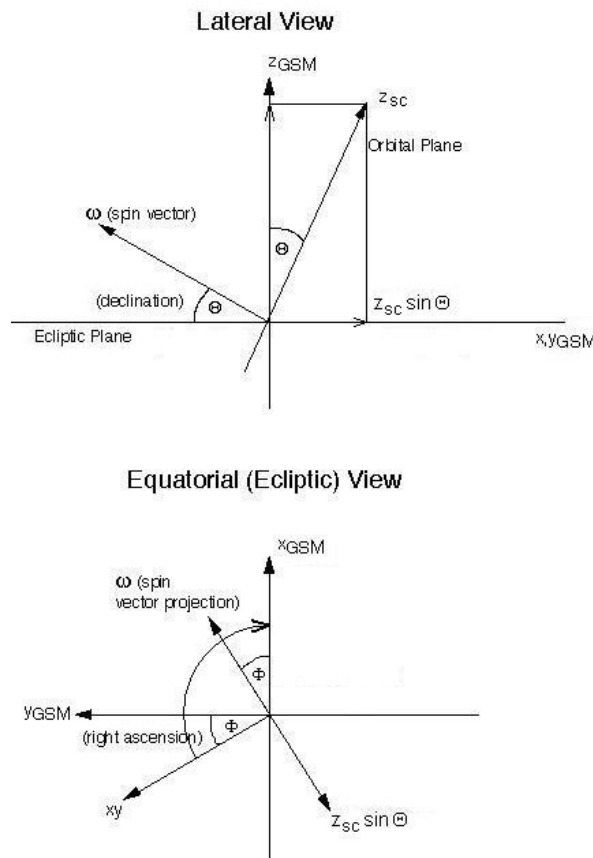


**Figure A1. Declination and right ascension angles of**

*the Polar satellite spin vector in the GSM coordinate system*

The transition from the satellite to the GSM coordinate system was carried out according to the following standard formulas:

$$E_z^{GSM} = E_z \cos \Theta,$$

$$E_x^{GSM} = E_{xy} \cos(90^\circ + \Phi) - (E_z \sin \Theta) \sin(90^\circ + \Phi),$$

$$E_y^{GSM} = E_{xy} \sin(90^\circ + \Phi) + (E_z \sin \Theta) \cos(90^\circ + \Phi),$$

$$E_x^{GSM} = -E_{xy} \sin \Phi - (E_z \sin \Theta) \cos \Phi,$$

$$E_y^{GSM} = E_{xy} \cos \Phi - (E_z \sin \Theta) \sin \Phi,$$

$$E_z^{GSM} = E_z \cos \Theta.$$

The longitudinal electric field component was calculated with a 6-second time resolution:

$$E_{||} = |E| \cos \theta$$

$$\theta = \arccos \frac{(\mathbf{B} \cdot \mathbf{E})}{|\mathbf{B}| |\mathbf{E}|}$$

Where  $\theta$  is the angle between the vectors of the magnetic ( $\mathbf{B}$ ) and electric ( $\mathbf{E}$ ) fields, found from the scalar product of the above vectors, presented in the GSM coordinate system.

**REFERENCES**

|  |  |
|--|--|
| <ol style="list-style-type: none"> <li>1. Arnoldy R. L., Engebretson M. J., Denton R. E., Posch J. L., Lessard M. R., Maynard N. C., Ober D. M., Farrugia C. J., Russell C. T., Scudder J. D., Torbert R. B., Chen S. H. and Moore T. E. Pc 1 waves and associated unstable distributions of magnetospheric protons observed during a solar wind pressure pulse. <i>J. Geophys. Res.</i> 2005, vol. 110, p. A07229. <a href="https://doi.org/10.1029/2005JA011041">https://doi.org/10.1029/2005JA011041</a>.</li> <li>2. Dovbnya B. V., Potapov A. S. Interpretation and analysis of the dispersed signals within 0.1–1.0 Hz in polar caps. <i>Issledovanija po geomagnetizmu, aeronomii i fizike Solntsa</i> [Investigations on Geomagnetism, Aeronomy and Solar Physics]. 1974, iss. 34, pp. 13-19 (in Russian).</li> <li>3. Dovbnya B. V., Potapov A. S. Possible origin of ultralow-frequency whistlers. <i>Cosmic Research.</i> 2004, vol. 42, pp. 349–353.</li> <li>4. Guglielmi A. V. MGD volny v okolozemnoi plazme [MHD waves in the near-terrestrial plasma], Moscow, Nauka Publ., 1979, p. 139 (in Russian).</li> <li>5. Guglielmi A. V., Troitskaya V. A. <i>Geomagnitnye pulsatsii i diagnostika</i></li> </ol> | <ol style="list-style-type: none"> <li><i>magnitosfery</i> [Geomagnetic pulsations and diagnostics of the magnetosphere]. Moscow, Nauka Publ., 1973, p. 208 (in Russian).</li> <li>6. Feygin F. Z., Nekrasov A. K., Pikkarainen T., Raita T., Prikner K. Pc1 pearl waves with magnetosonic dispersion. <i>J. Atmosph. Solar-Terr. Phys.</i> 2007, vol. 69. pp. 1644–1650. <a href="https://doi.org/10.1016/j.jastp.2007.01.019">https://doi.org/10.1016/j.jastp.2007.01.019</a>.</li> <li>7. Fraser B. J., Loto'aniu T. M., Singer H. J. The influence of wave-particle interactions on relativistic electron dynamics during storms. In: <i>Magnetospheric ULF Waves: Synthesis and New Directions. Geophys. Monogr. Ser.</i> 2006, vol. 169, ed. by K. Takahashi et al. AGU. Washington. D.C., pp. 195–212.</li> <li>8. Fukunishi H., Toya T., Koike K., Kuwashima M., Kawamura N. Classification of hydromagnetic emissions based on frequency-time spectra. <i>J. Geophys. Res.</i> 1981, vol. 86, no. A11, pp. 9029–9039. <a href="https://doi.org/10.1029/JA086iA11p09029">https://doi.org/10.1029/JA086iA11p09029</a>.</li> </ol> |
|--|--|

9. Harvey P., Mozer F. S., Pankow D., Wygant J., N. Maynard C., Singer H., Sullivan W., Anderson P. B., Pfaff R., Aggson T., Pedersen A., Fälthammar C. - G., Tanskannen P. The electric field instrument on the Polar spacecraft. *Space Sci. Rev.* 1995, vol. 71, pp. 583– 596. <https://doi.org/10.1007/BF00751342>.
10. Kangas J., Aikio A., Olson J.V. Multistation correlation of ULF pulsation spectra associated with sudden impulses. *Planet. Space Sci.* 1986, vol. 34, no. 6, pp. 543–553. [https://doi.org/10.1016/0032-0633\(86\)90092-9](https://doi.org/10.1016/0032-0633(86)90092-9).
11. Mann I. R., Usanova M. E., Murphy K., Robertson M. T., Milling D. K., Kale A., Kletzing C., Wygant J., Thaller S., Raita T. Spatial localization and ducting of EMIC waves: Van Allen Probes and ground-based observations. *Geophys. Res. Letters.* 2014, vol. 41, no. 3. <https://doi.org/10.1002/2013GL058581>.
12. Marmet P. New digital filter for analysis of experimental data. *Rev. Sci. Instrum.* 1979, vol. 50, no. 1, pp. 79–83.
13. Moore T. E., Chappell C. R., Chandler M. O., Fields S. A., Pollock C. J., Reasoner D. L. Young D. T., Burch J. L., Eaker, Waite Jr J. H., McComas D.J., Nordholdt J. E., Thomsen M. F., Berthelier J. J., Robson R. The Thermal Ion Dynamics Explorer and Plasma Source Instrument. *Space Sci. Rev.* 1995, vol. 71, pp. 409– 458. <https://doi.org/10.1007/BF00751337>.
14. Olson J. V., Lee L. C. Pc1 wave generation by sudden impulses. *Planet. Space Sci.* 1983, vol. 31, pp. 295–302. [https://doi.org/10.1016/0032-0633\(83\)90079-X](https://doi.org/10.1016/0032-0633(83)90079-X).
15. Parkhomov V. A., Zastenker G. N., Riazantseva M. O., Tsegmed B., Popova T. A. Bursts of geomagnetic pulsations in the frequency range 0.2-5 Hz excited by large changes of the solar wind pressure. *Cosmic Research.* 2010, vol. 48, pp. 86–100. <https://doi.org/10.1134/S0010952510010077>.
16. Pilipenko V. A., Polozova T. L., Engebretson M. Space-time structure of ion-cyclotron waves in the topside ionosphere as observed onboard the ST-5 satellites. *Cosmic Research.* 2012, vol. 50, pp. 329–339. <https://doi.org/10.1134/S0010952512050048>.
17. Russell C. T., Snare R. C., Means J. D., Pierce D., Dearborn D., Larson M., Barr G., Le G. The GGS Polar magnetic field investigation. *Space Sci. Rev.* 1995, vol. 71, pp. 563– 582. <https://doi.org/10.1007/BF00751341>.
18. Scudder J., Hunsacker F., Miller G., Lobell J., Zawistowski T., Ogilvie K., Keller J., Chornay D., Herrero F., Fitzenreiter R., Fairfield D., Needell J., Bodet D., Googins J., Kletzing C., Torbert R., Vandiver J., Bentley R., Fillius W., McIlwain C., Whipple E., Korth A. Hydra-A 3-dimensional electron and ion hot plasma instrument for the POLAR spacecraft of the GGS mission. *Space Sci. Rev.* 1995, vol. 71, pp. 459– 495. <https://doi.org/10.1007/BF00751338>.
19. Thorne R. M., Horne R. B., Jordanova V. K., Bortnic J., Glauert S. A. Interaction of EMIC waves with thermal plasma and radiation belt particles. In: *Magnetospheric ULF Waves; Synthesis and New Directions, Geophys. Monogr. Ser.* 2006, vol. 169, pp. 213–223. Edited by K. Takahashi, P. J. Chi, R. E. Denton and R. L. Lysak. American Geophysical Union, Washington, D. C.
20. Tsegmed B. Generation of a burst of geomagnetic pulsations in the 1–3 Hz frequency range in the daytime sector as a result of dramatic increases in the solar wind dynamic pressure. *Geomagn. Aeron.* 2011, vol. 51, no. 8, pp. 1138–1145. <https://doi.org/10.1134/S0016793211080305>.